

# The Brown Dwarf Mass Function from Pixel Microlensing

E.A. Baltz<sup>1</sup> and J. Silk<sup>2</sup>

<sup>1</sup>*ISCAP, Columbia Astrophysics Laboratory, 550 W 120th St., Mail Code 5247, New York, NY 10027, USA*

<sup>2</sup>*Nuclear and Astrophysics Laboratory, Keble Road, Oxford OX1 3RH*

Accepted Received

## ABSTRACT

We argue that gravitational microlensing is a feasible technique for measuring the mass function of brown dwarf stars in distant galaxies. Microlensing surveys of the bulge of M31, and of M87 in the Virgo cluster, may provide enough events to differentiate the behaviour of the mass function of lenses below the hydrogen burning limit (though we find that M87 is a more favourable target). Such objects may provide a significant supply of baryonic dark matter, an interesting possibility for the study of galactic dynamics. Furthermore, these systems have different metallicities than the solar neighbourhood, which may affect the mass function. These considerations are relevant in the context of star formation studies.

**Key words:** gravitational lensing — stars: low mass, brown dwarfs — cosmology:observations — dark matter — galaxies:haloes

## 1 INTRODUCTION

Gravitational microlensing, by which dark objects are detected by their magnification of bright sources being monitored, is a rapidly growing field, with many applications in astrophysics. Using microlensing to find dark objects in the halo of the Milky Way was first proposed by Paczyński (1986), and elaborated by Griest (1991). Several groups have extended the possibilities of microlensing by the so-called pixel technique (Crofts 1992; Baillon et al. 1993), where source stars are not resolved due to the high degree of crowding. However, successive images can be analysed, usually by taking image differences, to uncover the brightenings due to variability in the individual sources, some of which will be due to microlensing. This technique has been applied successfully by several collaborations (Tomaney & Crofts 1996; Alcock et al. 1999a,b; Woźniak 2000). Previously, it has been difficult to extract physical information from these pixel microlensing lightcurves because of a degeneracy in the lightcurve shape with magnification. The method of Gondolo (1999) for measuring the optical depth in pixel microlensing without knowledge of the magnification in an event has been extended to measurements of the mass function of lenses (Baltz 2000). In this paper we show how to apply this technique to measurements of the low-mass end of the stellar mass function, as has been done in classical microlensing surveys for brown dwarfs (Zhao, Spergel & Rich 1995) and planetary-mass objects (Alcock et al. 1998) in our own galaxy. We hope to extend such limits to distant galaxies as well.

## 2 BROWN DWARFS

Brown dwarfs are defined to lie in the mass range between the hydrogen-burning limit ( $75 M_{\text{Jup}}$ ) and the deuterium burning threshold ( $13 M_{\text{Jup}}$ ;  $1M_{\odot} = 1047M_{\text{Jup}}$ ). A theoretical review of these objects is given by Chabrier and Baraffe (2000). Radial velocity searches have detected both brown dwarfs and giant planets from  $75M_{\text{Jup}}$  to  $0.25M_{\text{Jup}}$  in orbits around solar-type stars. The observational situation for brown dwarfs is reviewed by Basri (2000). Studies of young star-forming regions have recently found evidence for isolated objects in the giant planet mass range ( $5 - 15M_{\text{Jup}}$ ) (Zapateo-Ossorio et al. 2000). Isolated brown dwarfs have also been reported in various star-forming regions (Lucas & Roche 2000; Hillenbrand & Carpenter 2000; Najita, Tiedo & Carr 2000). The frequency of such objects is not known, but they seem to be sufficiently numerous that the IMF must certainly continue from the hydrogen burning limit to the giant planet regime, and could either be flat, exhibit a weak power law decline, or even rise below the brown dwarf limit.

Observations of isolated brown dwarfs and giant planets are necessarily focussed on searching in star-forming regions, via the technique of infrared imaging. We show here that gravitational microlensing provides a potentially powerful technique for exploring the initial mass function of brown dwarfs in distant galaxies.

We investigate several possible mass functions for this type of object, below the hydrogen burning limit. Our proposed method will not be able to distinguish fine features in the mass function, so we investigate several toy mass functions. It is the gross features of the mass function that we are immediately concerned with, and simple model mass func-

arXiv:astro-ph/0012325v2 21 Feb 2001

tions will suffice. We consider the class of mass functions (taking  $M$  in units of  $M_{\odot}$ , and with arbitrary normalisation)

$$\log \left( \frac{dN}{d \log M} \right) = - [A \log M + B (1 - \log M)^2], \quad (1)$$

where  $A$  and  $B$  are free parameters (note that  $B = 0$  corresponds to a pure power-law mass function  $dN/d \log M \propto M^{-A}$ ). These mass functions agree at ten solar masses, and taking  $A = 1.35$ , have the Salpeter (1955) slope at ten solar masses. This prescription ensures that the mass functions produce equal light, as most of the visible light from stellar populations comes from massive stars, heavier than the sun. The uncertainty in the population thus lies in the mass to light ratio, not in the total light, which is as it should be.

Taking  $B = 0.25$  gives a mass function with approximately the Salpeter (1955) slope down to  $0.02M_{\odot}$ . This model has a large amount of stellar mass below the hydrogen burning limit, indicating a large amount of baryonic dark matter locked up in brown dwarf stars. Taking  $B = 0.32$  gives a mass function turning over at around  $0.08M_{\odot}$ , similar to the Miller–Scalo (1979) mass function. Lastly, we take  $B = 0.48$ , giving a mass function turning over at around  $0.4M_{\odot}$ , similar to that of Gould, Bahcall & Flynn (1996). This model has the least amount of baryonic dark matter.

### 3 SURVEYS OF DISTANT GALAXIES

Pixel microlensing surveys of large distant galaxies are quite attractive for learning about both the dynamical properties of the systems and the populations of objects from which they are made. We will discuss two possible targets to illustrate the capabilities of this technique with ground and space based telescopes.

A pixel microlensing survey of M31, the Andromeda Galaxy, is quite feasible using a three-meter class ground based telescope. This large spiral galaxy is about 725 kpc distant, and is the nearest large galaxy to the Milky Way. We are primarily interested in the bulge of this galaxy, as it affords the densest star fields and the largest optical depth for star–star lensing. However, finite source size effects for this target would require nearly continuous monitoring for reasonable sensitivity at low masses to be achieved, so we will not consider M31 further.

Using a space-based telescope, the reach of the pixel technique is much longer. The giant elliptical galaxy M87, at the center of the Virgo cluster at a distance of about 15 Mpc, is well within the reach of a pixel microlensing survey by the Hubble Space Telescope (HST). We take a mass model based on the work of Tsai (1993),

$$\rho(r) = 3.8 \left[ 1 + \left( \frac{r}{\text{kpc}} \right)^2 \right]^{-\alpha} M_{\odot} \text{ pc}^{-3}, \quad (2)$$

$$\alpha = \max \left[ 1, 1 + 0.275 \log \left( \frac{r}{\text{kpc}} \right) \right]. \quad (3)$$

The Advanced Camera for Surveys (ACS) is an ideal instrument for this type of observation. The future NGST, planned as an eight meter class space telescope, will allow a much more thorough survey, with better statistics. For

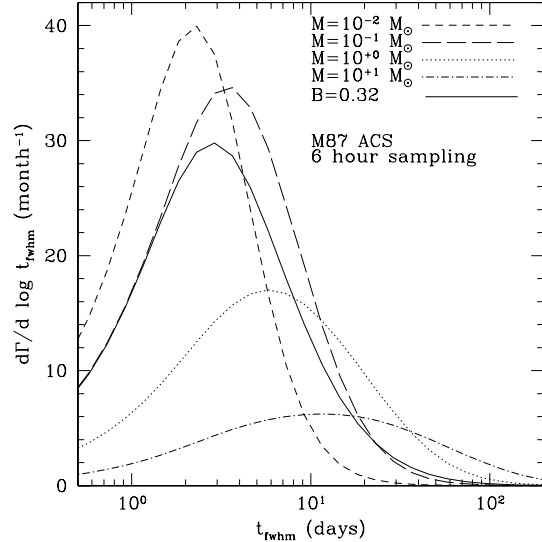


**Figure 1.** Self-lensing event rate towards M87 bulge with ACS on HST. The sample spacing is four times daily. There is a much lower sensitivity to lenses below about  $10^{-2} M_{\odot}$ . We illustrate delta function mass functions, together with the  $B = 0.32$  Miller–Scalo type mass function.

both telescopes we assume exposures of thirty minutes (for the HST ACS, this is possible in one orbit), taken every six hours. More frequent sampling is punishing in that fewer events are detected with the same telescope resources (say 30 orbits for HST), though smaller masses can be probed. Less frequent sampling may allow more events to be detected with the same telescope resources, but at the cost of the low-mass sensitivity that we desire for this program. For our purposes, six-hour sampling is about ideal, though with the NGST there is more room to take a larger sample spacing. We show the event rates for these two telescopes below, in Figs. 1 and 2 respectively (Baltz & Silk 2000). Rates for the NGST assume a field of view  $4'$  square, with 50% more throughput than the HST ACS, and nine times the collection area. In all cases in this paper, we assume that seven samples above  $2\sigma$  must be collected, as Criteria A of Alcock et al. (2000).

### 4 MEASURING THE MASS FUNCTION

For each pixel microlensing event, we make in effect two measurements. These are the flux increase at maximum  $\Delta F_{\text{max}}$ , and the full-width at half maximum time,  $t_{\text{fwhm}}$ . As Woźniak & Paczyński (1997) have clearly shown, even in the classical microlensing case, the shape of the lightcurve does not give much more information than these two parameters. However, in the classical microlensing case, an additional measurement, that of the unlensed flux of the source star, is also made, allowing an accurate determination of the magnification of the event.

The Einstein times of events have been used to estimate the optical depth to microlensing, and also to estimate the masses of the lenses. However, to make a good estimate of the Einstein time from a microlensing event, both  $t_{\text{fwhm}}$

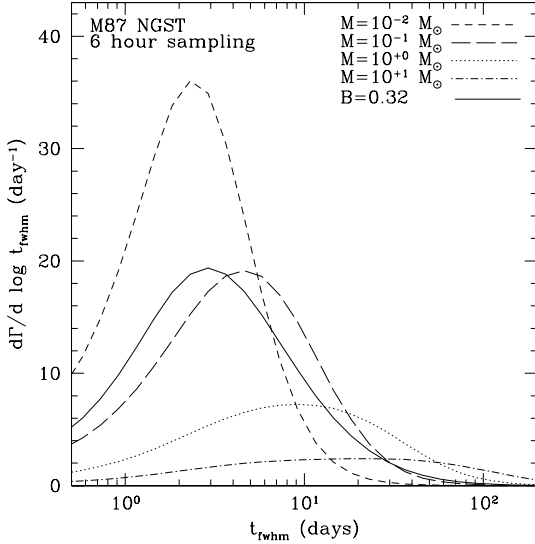


**Figure 2.** Self-lensing event rate towards M87 bulge with NGST. The sample spacing is four times daily. The sensitivity drops considerably below about  $10^{-3} M_{\odot}$ . The mass functions are the same as in Fig. 1.

and the magnification are required. We thus seek a different characteristic of events. The time-scale  $t_{\text{fwhm}}$  is problematic, as it strongly depends on the unknown magnification. We instead follow Gondolo (1999) and use the quantity  $\omega_F = \Delta F_{\text{max}} t_{\text{fwhm}}$ , which is effectively the Einstein time multiplied by the flux of the source star. This quantity is easily measured from pixel microlensing events. We choose to further normalize by dividing by the surface brightness fluctuation flux ( $\bar{F} \propto 10^{-0.47m}$ ),

$$t_F = \frac{\Delta F_{\text{max}} t_{\text{fwhm}}}{\bar{F} \sqrt{3}}. \quad (4)$$

The SBF flux  $\bar{F}$  is measured by characterizing the pixel-to-pixel variations of the surface brightness of a galaxy image (Tonry & Schneider 1988). This normalisation gives the approximate relation, with  $\beta$  being the event’s minimum impact parameter in Einstein units,

$$t_F = t_E 10^{-0.4(m-\bar{m})} \left( 1 - \frac{7}{3} \beta + \frac{311}{72} \beta^2 + O(\beta^3) \right) \quad (5)$$

when  $\beta \ll 1$ , or equivalently, at high magnification. Gondolo (1999) showed how to measure the optical depth to microlensing using this time-scale. We will use an extension of that method, described in more detail in Baltz (2000), to constrain the mass function of the lenses, in this case brown dwarfs. The method is based on producing a weighted histogram of event rate with flux time-scale  $t_F$ . Differentially, we want to study the dimensionless rate

$$N_F = t_F \frac{d\Gamma}{d \log t_F}, \quad (6)$$

given a delta-function mass function. The quantity  $N_F$  then encodes the response of a microlensing survey to lenses of a given mass, effectively the number of events expected per decade in time-scale when monitoring for a time equal to the event time-scale. Equivalently, this quantity is closely

related to the optical depth contributed by lenses producing events at a specific time-scale.

For comparison, we can form quantities analogous to  $N_F$  using the other relevant time-scales, namely the Einstein time ( $N_E$ ) and the full-width at half maximum time ( $N_{t_{\text{fwhm}}}$ ). Their definitions exactly mimic Eq. 6.

At fixed mass, one would naively think that the Einstein time is most useful, as the distribution is the narrowest of the three. However, the Einstein time can be measured only rarely. Furthermore, we find that the shape of the rate distribution with the Einstein time is sensitive to the exact details of the cuts used to define events. Interestingly, the shape of the rate distribution with the flux time is much less sensitive to the exact definition of an event, which is clearly a desirable feature. This happens because changing the definition of an event usually amounts to changing the minimum value of the flux increase at maximum. This will simply change the short time-scale end of the  $t_F$  distribution, leaving the peak shape intact in most cases. This point is further explored in Baltz (2000). Thus, it seems that the time-scale  $t_F$  is perhaps preferable to the Einstein time in extracting the parameters of the source–lens system. In Figs. 3 and 4, we display the function  $N_F$ , given delta-function mass functions. Effectively, these are the smoothing kernels over which the true mass function can be measured. In Fig. 5 we plot the function  $N_E$ , based on the Einstein time-scale, for the same exact parameters as for the ACS in Fig. 3. As is clearly evident, the function  $N_E$  is more sensitive *near its peak* than  $N_F$  to changing the effective threshold, as is the case for changing the sampling strategy. Thus the discussion in this paragraph is validated: even if  $t_E$ , and thus  $N_E$ , were measurable,  $N_F$  is preferred in cases where there is a high sensitivity to the threshold for events.

The universality of the shape is broken by two effects: finite source size and finite time sampling. The primary effect of the finite source size is that the magnification is bounded by the fact that the source stars are not point sources. This effect is obviously more pronounced for smaller Einstein rings, and thus for smaller masses. A finite time sampling implies a minimum event time-scale that can be detected. Lower mass lenses of course produce shorter events, thus more of the low-mass events are missed. The finite total observing time would also subtract very long events, but for our purposes, this is not a concern, as we are interested in the short events due to  $0.01\text{--}0.1 M_{\odot}$  stars.

## 5 DISCUSSION

We now illustrate the full  $N_F$  distribution, integrated over the simple mass function discussed in Sec. 2. As discussed previously,  $N_F$  for a single mass acts as a smoothing filter for the mass function. We show the results for the HST ACS in Fig. 6 and the NGST in Fig. 7. The pure Salpeter mass function has a peak at the shortest time-scale, the flattened models (Miller-Scalo and Salpeter with cutoff) has a longer peak, and the GBF-type model has the longest peak time-scale. With these surveys, the statistics should be sufficient to distinguish these models. We should state that the normalisation alone is probably insufficient to distinguish models, but the position in time-scale of the peak of the rate distribution is quite robust. In fact, we have adjusted the

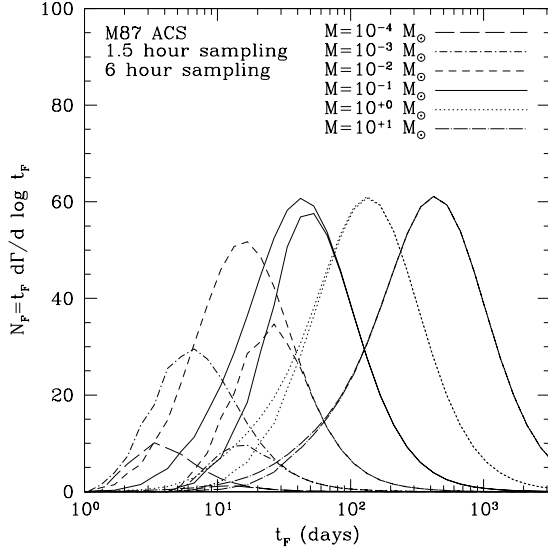


**Figure 3.** Dimensionless rate  $N_F$  for ACS on HST. The curves are, left to right, for lenses of a single mass:  $10^{-4}, -3, -2, -1, 0, 1 M_\odot$ . Samples are taken every 1.5 hours in the top curves, with the lower curves sampling every six hours. With six hour sampling, the sensitivity begins to decline at masses less than  $10^{-1} M_\odot$ , and is quite low below  $10^{-2} M_\odot$ .

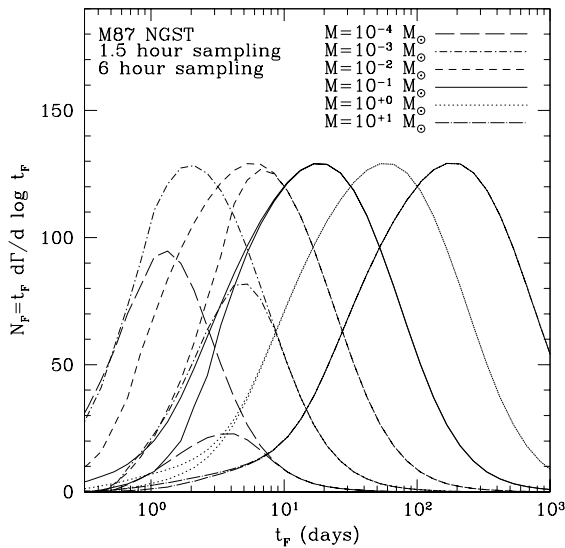


**Figure 4.** Dimensionless rate  $N_F$  for NGST. The curves are analogous to those in Fig. 3. With six hour sampling, the sensitivity only begins to seriously decline at masses less than  $10^{-2} M_\odot$ .

normalisation of the  $B = 0.3$  and  $B = 0.75$  models so that the peak rates agree, in order to compare the time-scales. For the surveys we consider, the peak time-scale differs by a factor of 2-3 between a mass function that is flat for substellar masses (Miller-Scalo), and one that is sharply declining at those masses (GBF). We note that mass functions that differ only below  $0.1 M_\odot$  will be quite difficult to distinguish, but for mass functions which begin to differ

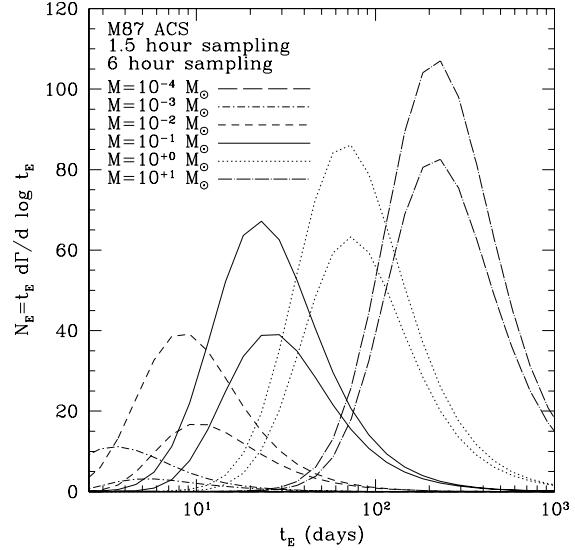


**Figure 5.** Dimensionless rate  $N_E$  for ACS on HST. The curves are analogous to those in Fig. 3, and in fact represent the same microlensing survey, with the time-scale  $t_E$  rather than  $t_F$ .

at around a solar mass, the microlensing technique is quite powerful.

We have shown that pixel microlensing can be a powerful tool for measuring the mass function of low mass and brown dwarf stars, less massive than the sun. Since this technique is effective to very large distances, we have a chance to learn something about the universal properties of brown dwarf mass functions.

## ACKNOWLEDGMENTS

We thank P. Gondolo, E. Kerins, N.W. Evans and the anonymous referee for useful conversations.

This paper has been produced using the Royal Astronomical Society/Blackwell Science L<sup>A</sup>T<sub>E</sub>X style file.

## REFERENCES

- Alcock C. et al., 1998, ApJ, 499, L9
- Alcock C. et al., 1999a, ApJ, 521, 602
- Alcock C. et al., 1999b, ApJS, 124, 171
- Alcock C. et al., 2000, ApJ, 542, 281
- Baillon P., Bouquet A., Giraud-Héraud Y. & Kaplan J., 1993, A&A, 277, 1
- Baltz E.A., 2000, PhD Thesis, Univ. California, Berkeley (<http://www.astro.columbia.edu/~eabaltz/thesis.html>)
- Baltz E.A., Silk J., 2000, ApJ, 530, 578
- Basri G., 2000, ARA&A, 38, 485
- Chabrier G. & Baraffe I., 2000, ARA&A, 38, 337
- Crotts A. P. S., 1992, ApJ, 399, L43
- Gondolo P., 1999, ApJ, 510, L29
- Gould A., Bahcall J.N. & Flynn C., 1996, ApJ, 465, 759
- Griest K., 1991, ApJ, 366, 412
- Hillenbrand L. and Carpenter J., 2000, ApJ (in press)
- Lucas P. and Roche P., 2000, MNRAS, 314, 858
- Miller G.E. & Scalo J.M., 1979, ApJS, 41, 513
- Najita, J. Tiedo G. and Carr J., 2000, ApJ (in press)

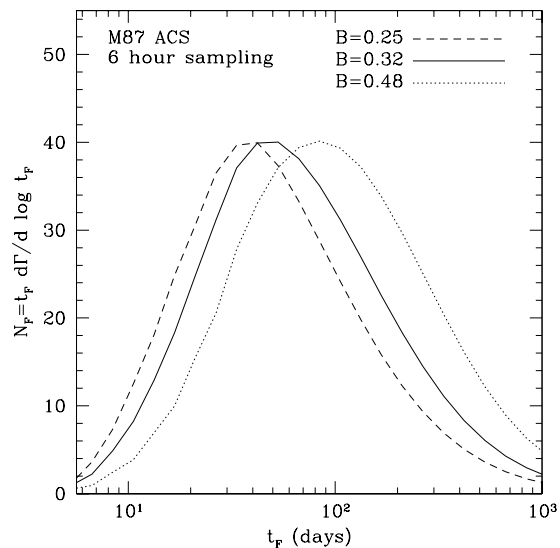


**Figure 6.** Mass functions with ACS on HST. We illustrate the measured  $N_F$  for the three basic mass functions. The normalisations of the  $B = 0.25$  and  $B = 0.48$  curves have been adjusted to compare the peak positions with the  $B = 0.32$  case.

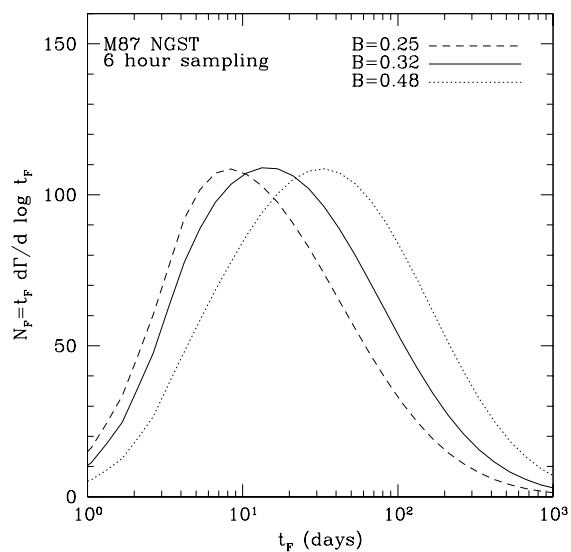


**Figure 7.** Mass functions with NGST. We illustrate the measured  $N_F$  for the three basic mass functions. The normalisations have been adjusted as in Fig.6

- Paczynski B., 1986, ApJ, 304, 1  
 Salpeter E.E., 1955, ApJ, 121, 161  
 Tomaney A.B. & Crots A.P.S., 1996, AJ, 112, 2872  
 Tonry J. & Schneider D.P., 1988, AJ, 96, 807  
 Tsai J.C., 1993, ApJ, 413, L59  
 Woźniak P., 2000, AcA, 50, 421  
 Woźniak P., Paczyński B., 1997, ApJ, 487, 55  
 Zapateo-Ossorio M. et al., 2000, Science (in press)  
 Zhao H., Spergel D.N. & Rich R.M., 1995, ApJ, 440, L13